NANO LETTERS

2007
Vol. 7, No. 6
1591−1597

Cancer Cells Assemble and Align Gold Nanorods Conjugated to Antibodies to Produce Highly Enhanced, Sharp, and Polarized Surface Raman Spectra: A Potential Cancer Diagnostic Marker

Xiaohua Huang,[†] Ivan H. El-Sayed,[‡] Wei Qian,[†] and Mostafa A. El-Sayed*[,†,§]

Laser Dynamics Laboratory, School of Chemistry and Biochemistry, Georgia Institute of Technology, Atlanta, Georgia 30332, Otolaryngology-Head and Neck Surgery, Comprehensive Cancer Center, University of California, San Francisco, California 94143, and University of California, Berkeley, California 94720

Received February 27, 2007; Revised Manuscript Received April 19, 2007

ABSTRACT

Human oral cancer cells are found to assemble and align gold nanorods conjugated to anti-epidermal growth factor receptor (anti-EGFR) antibodies. Immnoconjugated gold nanorods and nanospheres were shown previously to exhibit strong Rayleigh (Mie) scattering useful for imaging. In the present letter, molecules near the nanorods on the cancer cells are found to give a Raman spectrum that is greatly enhanced (due to the high surface plasmon field of the nanorod assembly in which their extended surface plasmon fields overlap), sharp (due to a homogeneous environment), and polarized (due to anisotropic alignments). These observed properties can be used as diagnostic signatures for cancer cells.

Gold nanorods are unique class of metal nanostructures that have been found to be very useful for biomedical and biological applications. They have two surface plasmon absorption bands,[1] a strong long wavelength band in the near-infrared region due to the longitudinal oscillation of the conduction band electrons, and a weak short wavelength band around 520 nm due to the transverse electronic oscillation.[2−7] The longitudinal absorption band is very sensitive to the aspect ratio of the nanorods. By increasing the aspect ratio (length divided by width), the longitudinal absorption maximum shifts to longer wavelength with an increase in the absorption intensity.[4−8] The longitudinal absorption band has a much higher sensitivity to the local dielectric environment than the absorption band of spherical nanoparticles.[6] Because of the enhanced surface electric field upon surface plasmon excitation, gold nanorods absorb and scatter electromagnetic radiation strongly. Using this enhanced, sensitive, and tunable optical absorption and scattering properties, gold nanorods have been used in optical sensing,[9,10] in biomedical imaging,[11−13] and in photothermal therapy.[11,14−16] In our previous study, antibody conjugated gold nanorods were demonstrated to be excellent contrast agents for both cancer cell diagnostics and for selective photothermal therapy in the near-infrared region and thus have potential use for in vivo applications.[11]

Gold nanorods also provide a novel type of surface enhanced Raman scattering (SERS) substrate.[17−24] The well developed synthesis of nanorods with different aspect ratios[25−27] provides the opportunity to tune the surface plasmon band to the excitation laser wavelength to obtain maximum enhancement. The presence of {110} facets, which is not present in gold nanospheres, is shown to have strong adsorption energies for adsorbed molecules.[18,28,29] It has been calculated that the surface electromagnetic field of rods is the highest compared with other shapes due to the rod's high curvatures (called "the lightning rod" effect).[30,31] In addition, rods like to assemble with overlapping surface plasmon fields that can be defined as field aggregates.[32−36] In fact, the extremely large surface Raman enhancement observed on plasmonic nanoparticles occurs because of the large electric fields in between assembled or aggregated particles.[18,37−40] This is found to be the cause of the greatly enhanced Raman signal on the order of 10^{14} for a single (not averaged) cross-section using single molecule techniques.[41]

* Corresponding author. E-mail: melsayed@gatech.edu. Telephone: 404-894-0292. Fax: 404-894-0294.
[†] Georgia Institute of Technology.
[‡] University of California, San Francisco.
[§] Miller Visiting Professor, University of California, Berkeley, California 94720.

10.1021/nl070472c CCC: $37.00
Published on Web 05/03/2007

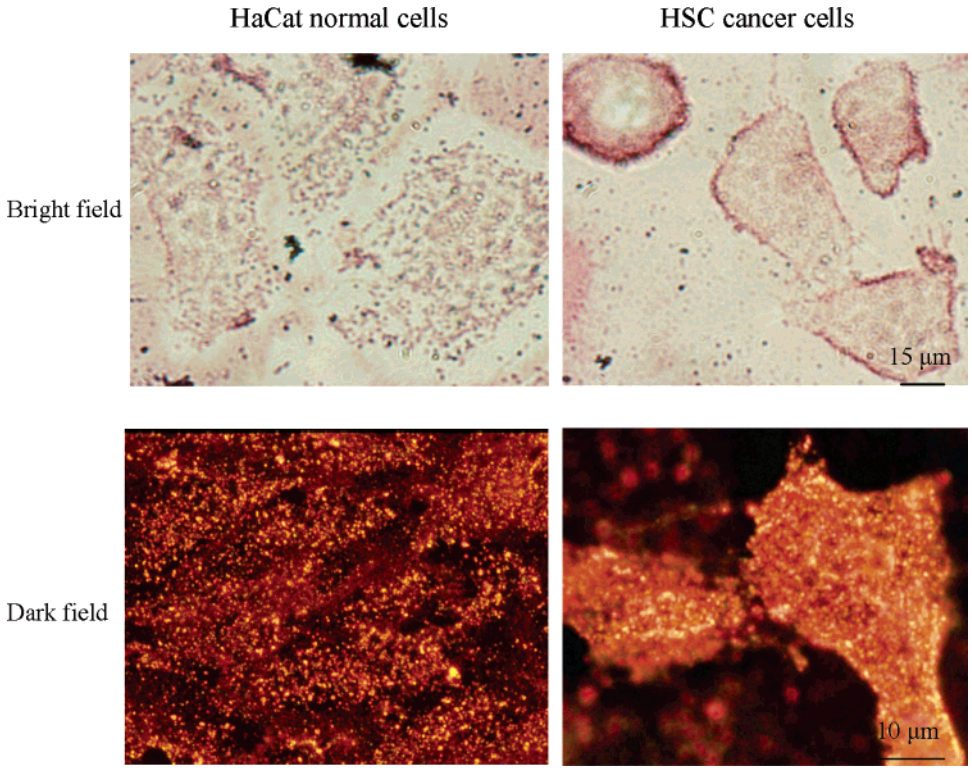

Figure 1. Bright and dark field images of anti-EGFR antibody conjugated gold nanorods on HaCat normal and HSC cancer cells. As we showed previously (refs 11, 69), dark field imaging is most appropriate for plasmonic nanoparticles targeting in nanobiology due to their enhanced and selective scattering properties.

Gold nanorods are potentially useful in SERS for biological species, especially for single cell studies. It is well-known that most biological molecules have small Raman scattering cross-sections that result in very weak signals. Resonance Raman when the laser frequency is in resonance with that of an electronic transition of a chromophore has frequently been used to get enhanced signals. However, photochemical damage frequently occurs when UV or visible lasers are used. In addition, interference from the fluorescence from some of these residues frequently limits the use of this technique to the study of the fluorescent chromophores. An alternative method is the enhancement of Raman scattering by the roughened metal surface, which is called surface enhanced Raman scattering (SERS).[42−44] Individual or aggregated gold and silver nanoparticles have been used as SERS substrates in living cell studies.[45−49] By using gold nanorods, one can use a near-infrared laser to obtain maximum enhancement by overlapping the absorption maximum with the laser wavelength without cell damage because DNA and proteins have no absorption in this region.

In the present study, gold nanorods having longitudinal absorption maximum at 800 nm are conjugated to monoclonal anti-epidermal growth factor receptor (anti-EGFR) antibodies. The antibody/gold conjugates are incubated with a normal skin cell line and an oral cancer cell line. The bright and dark field images, single cell absorption, and surface enhanced Raman spectra of molecules within the surface plasmon fields of the gold nanorods of normal and cancer samples are measured and compared. The polarized Raman spectra of these samples are also measured. The strong, sharp, and polarized Raman spectra of the CTAB (nanorod capping molecules) observed in the cancer cell samples, but not in the healthy cell samples, strongly suggest that gold nanorods are aggregated in an aligned assembly on the surface of the cancer cells while they are randomly and individually distributed in the healthy cell samples.

The synthesis of gold nanorods and their antibody conjugation have been described in detail before.[11] Gold nanorods with an aspect ratio of 3.9, the longitudinal absorption maximum of which are around 800 nm, are used in this experiment. The nanorods are coated with poly(styrene sulfonate) (PSS, MW = 18 000, Polysciences Inc.) polyelectrolyte before conjugation to anti-EGFR antibodies (Sigma) to reverse the surface charge of the nanorods.[50] The antibodies are bound to PSS polyelectrolyte coated nanorods at pH = 7.4 by noncovalent interactions.[51,52] The anti-EGFR antibody conjugated gold nanorods are stored in PBS buffer at 4 °C.

One type of nonmalignant epithelial cell line, HaCaT (human keratinocytes) and one type of malignant epithelial cell line, HSC 3 (human oral squamous cell carcinoma), are cultured on cover slips in Dulbecco's modification of Eagle's medium, (DMEM, Cellgro) plus 10% fetal bovine serum (FBS, Gem Cell) at 37 °C under 5% CO_2. The cells on the cover slips are rinsed with PBS buffer and then immersed into the anti-EGFR conjugated nanorods solution (1nM) for 30 min at room temperature. After the nanorod incubation, the cells are rinsed with PBS buffer, fixed with paraformaldehyde and sealed with another cover slip.

The bright and dark field images are taken under an inverted Olympus IX70 microscope. Bright field images are

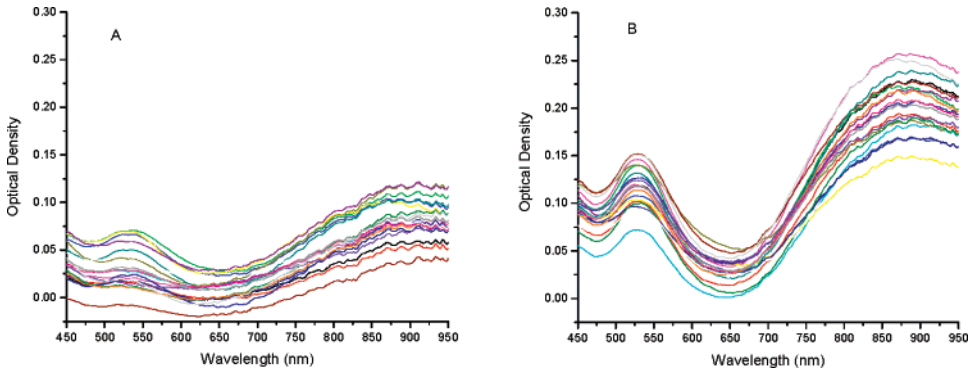

Figure 2. Surface plasmon resonance microabsorption spectra of anti-EGFR/gold nanorods from 20 different single cells for HaCat normal (A) and HSC cancer cells (B).

taken with a 60× objective. For dark field imaging, a dark field condenser (U−DCW) with a numerical aperture between 0.9 and 1.2 is used to deliver a narrow beam of white light from a tungsten lamp to the sample. A 100×/1.35 oil Iris objective (UPLANAPO) is used to collect only the scattered light from samples. In this mode, samples with highly scattering property are shown as a bright object in a dark background.

The Raman spectra are obtained with a Holoprobe series 5000 microspectrometer (Kaiser Optical Systems, Inc., Ann Arbor, MI) in a 180° reflective configuration using a 50× objective. The excitation wavelength is 785 nm from a diode laser, which is in resonance with the surface plasmon absorption of the gold nanorods. The spectral resolution in the Raman experiments is 5 cm^{-1} and the laser power used is 25 mW. Each spectrum is obtained in 10 s collection time with six accumulations. For the polarized Raman experiment, the cover slip with the cells is fixed on the center of a rotation stage with rotation resolution of 1°. The polarized Raman spectra are obtained by rotating the sample with respect to the electric field of the excitation laser at different angles with an interval of 20°.

Gold nanorods conjugated with anti-EGFR monoclonal antibodies are known to preferentially bind to human oral cancer cells over normal cells.[11] This difference in affinity can be seen in the microscopic images in Figure 1 and the absorption spectra from single cells in Figure 2. In bright field mode, gold nanorods can be identified by the weak red color images due to the binding of the antibodies onto the gold surface and the antibodies onto the cell surface. However, in dark field mode, gold nanorods strongly scatter the enhanced red light because the surface plasmon oscillation has a frequency in the near-infrared region. Most of the nanorods bind to the cancer cell surface while they are randomly distributed in the different environments present in the sample containing the healthy cells.

Figure 2 shows that the absorption spectrum of gold nanorods in the sample incubated with the normal cells is broader than that on the cancer cells. This suggests that the environments of the different rods in the two samples are different and the absorption maxima of their surface plasmon oscillations are at different wavelength. The sharper absorption spectrum of the cancer samples suggests that the gold nanorods are more homogenously dispersed on the cancer cell surface. The higher intensity of the nanorods on the cancer cells indicates a higher affinity of the nanorods to these cells. These differences in the absorption spectra of gold nanorods arise because the gold nanorods bind to the overexpressed EGFR present on the surface of cancer cells.

Figure 3 shows the surface enhanced Raman spectra from different cells for both normal (A) and cancer (B) cells after the incubation with anti-EGFR/Au nanorod conjugates. Over 20 cells for both normal and cancer cells are measured. For normal cells, 80% cells are found to give no Raman spectra and 20% cells give only weak spectra from the CTAB (hexadecyltrimethylammonium bromide) capping molecules (see Figure 5 for peak assignments). For the cancer cells, about 90% show very strong signals from not only the CTAB capping molecules but also from the PSS coating molecules and the anti-EGFR antibodies (See Figure 5 for peak assignments). 10% of the cancer cells show only the strong CTAB signals. Figure 3 shows five spectra for each cell line.

From Figure 2, it can be seen that the absorption intensity of the cancer cell sample is twice as strong as the healthy cell sample. This does not however give any information about the difference in the concentrations because we have no information about the difference in the plasmon enhancement factors due to the nanorod assembly on the cancer cells. The strong Raman spectrum observed in the cancer cells could very well result from a small fraction of the rods on the cancer cell surface that has a very strong surface plasmon field overlapping and rod alignment.

The overlapping of the surface plasmon fields of the different rods on the cancer cell surface results from the binding of the antibodies to its overexpressed EGFR. EGFR is overexpressed in many carcinomas on the order of 10^4-10^6 receptors/cell,[53] exists in preformed dimmers[54,55] and is clustered on the cell surface in groups of 10−50 receptors.[56] Crystallization[57] and FRET[54,58] studies indicate the receptors exist in preformed dimers with the two EGFR monomers spaced less than 8 nm apart. This is much smaller than the decay distance of the nanorod surface plasmon fields, which can be on the order of the nanorod size.

Thus nanorods attached to EGFR antibodies will be brought into close proximity on the cell surface. This organization (or aligned assembly) of the gold nanorods

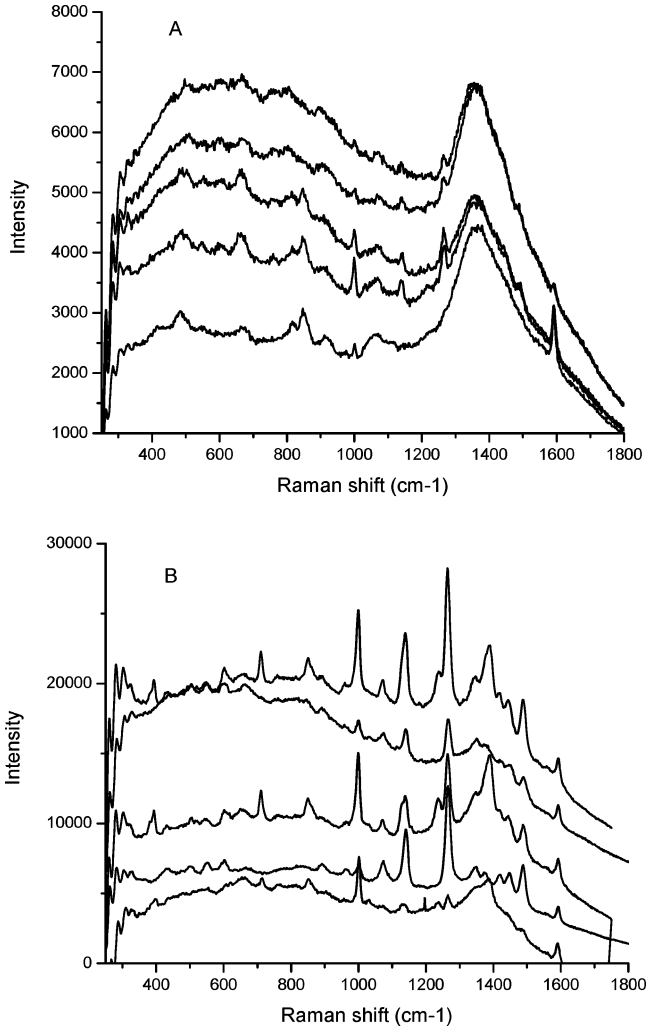

Figure 3. SERS of anti-EGFR antibody conjugated gold nanorods incubated with the HaCat normal cells (A) and HSC cancer cells (B). Raman spectra from five cells for each cell line are shown. The bottom spectra from the cancer cell samples are stronger, sharper, and better resolved, suggesting the potential of using surface enhanced Raman spectroscopy as a molecular type imaging for the diagnostics of cancer.

allows them to have overlapping surface plasmon fields that bathe some of the molecules in the system, giving them strong and sharp Raman spectra. The nonspecific binding of gold nanorods to normal cells results in randomly distributed nanorods on the cell surface and on the substrate. This makes the nanorod density level and the overlapping surface plasmon fields in the normal cell sample much lower and more heterogeneous than in the cancer cell sample. These spectral fingerprint differences can very well be used as molecular diagnostics for the cancer cells.

Further support of the presence of more organized (or aligned) assembly of the gold nanorods on the surface of the cancer cells is obtained from the results of the polarized micro-Raman experiments shown in Figure 4A. In this Figure, the apparent polarization dependence of the SERS from anti-EGFR conjugated gold nanorods on a single cancer cell is shown. Because the initial orientation of the gold nanorods relative to the direction of the electric field of the incident laser is unknown in this experiment, the direction of the sample that gives the maximum CTAB Raman scattering around 1265 cm^{-1} is set to be 0° in the polarized Raman spectrum. The SERS spectra are recorded in the range from −90° to 90° with every 20° of rotation of the sample on the rotation stage relative to the incident laser polarization. To clearly observe the variation of the intensity of the Raman peak as a function of sample rotation, the specific peaks of CTAB band at 1265 cm^{-1}, which is the strongest in Figure 4A, is selected and shown in Figure 4B. From Figure 4B, the anisotropic nature can be seen with the minimum intensity value of about 0.4 that of the maximum intensity. Figure 4C shows the peak intensity of the 1265 cm^{-1} band as a function of rotation angle from −90° to 90°. It can be seen that the Raman intensity decreases as the rotation angle changes from 0° to 90° or 0° to −90°. Obviously, the change in the intensity of the 1265 cm^{-1} band from the Raman scattering of the CTAB molecules as a function of rotation angle is due to the anisotropic orientation of the average CTAB molecules relative to the incident laser polarization. Because the molecules are attached to the gold nanorods, which enhance their Raman spectra, the nanorods themselves must be aligned to give an anisotropic orientation in space, which the electric field direction of the laser reveals. Thus some (or all) the EGFR molecules on the cancer cell surface bind to the anti-EGFR antibodies in such a manner that results in the observed anisotropic orientation of the attached gold nanorods.

To assign the Raman bands of the anti-EGFR conjugated gold nanorods on the cell surface, the surface enhanced Raman spectra of the molecules present in the sample are compared with the spectra of the CTAB capping molecules, the anti-EGFR antibodies, and PSS powder. These spectra are compared with the observed surface enhanced Raman spectrum of the cancer cell sample in Figure 5.

The CTAB capping molecules show very strong SERS signals (see Figure 5B). The band assignments made here are based on the studies of El-Sayed et al.,[17] Pemberton et al.,[59] and Murphy et al.[60] The Raman lines at 1076 and 1140 cm^{-1} are assigned to υ_{asym} (C−C) and υ_{sym}(C−C) vibrations,[59] respectively. The strongest line at 1265 cm^{-1} is assigned to the δ(C−H) vibrations of the $-CH_2-N^+(CH_3)_3$ group.[17] The two weak bands at 1446 and 1485 cm^{-1} are both assigned to CH_2 bending vibrations.[17] The 1000 cm^{-1} line is assigned to the C−N stretch in the head group.[60]

After the adsorption of anti-EGFR antibody directly onto the rod surface, some new peaks appear. From the difference spectra of (A) and (B) shown in Figure 5D, it can be seen that the antibodies show strong peaks at 670, 898, and 1003 cm^{-1}. The 670 cm^{-1} band is attributed to C−S stretching vibrations in the cystine residues.[59−61] The 898 cm^{-1} can be assigned to the C−C stretching in the glycine and the 1003 cm^{-1} to ring C−C stretch vibrations in the phenylalanine redisues.[61−63] There is also a weak peak at 510 cm^{-1}, which is probably due to the S−S stretching vibrations in the cystine residues.[61] There are no observed Raman signals from the antibody molecules alone in the absence of gold nanorods. The PSS charge reversing polyelectrolytes have a very strong

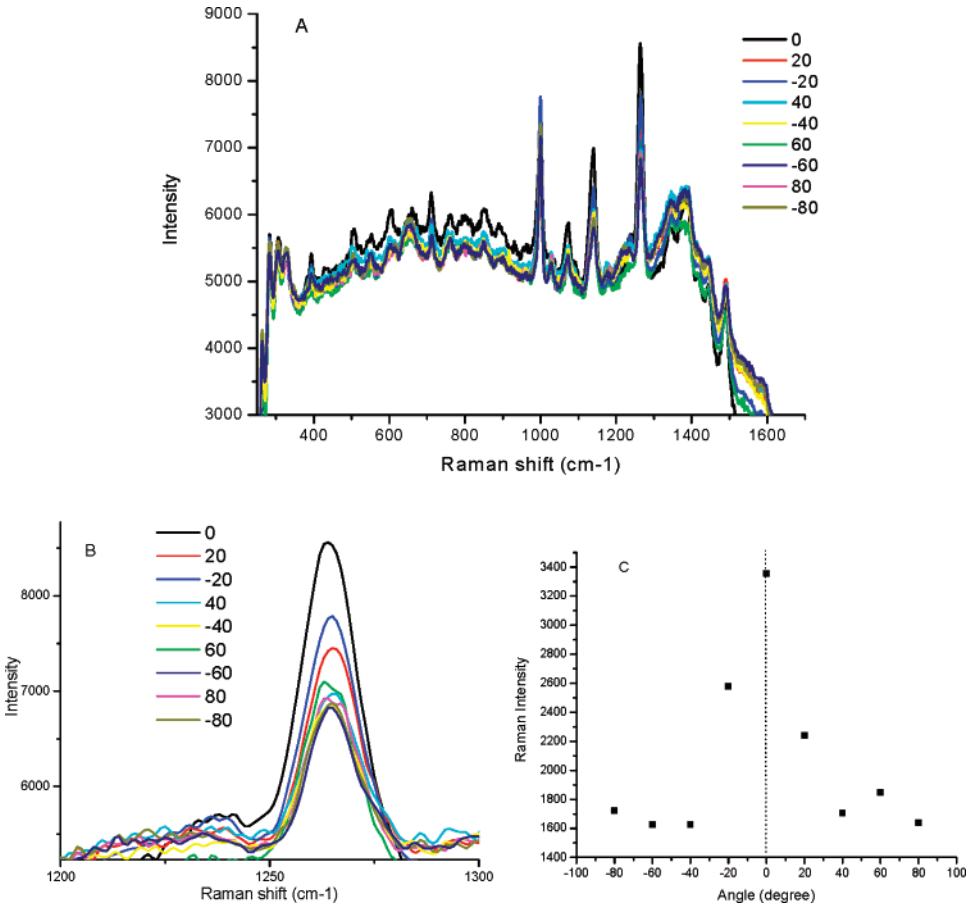

Figure 4. Polarization property of SERS of anti-EGFR conjugated gold nanorods on the HSC cancer cells (due to the weakness of the signal, no polarized spectrum from the healthy cells could be recorded). (A) The polarized Raman spectra at different angles relative the electric field of the excitation laser; (B) the zoom in region of the strong band at 1265 cm^{-1} of the gold nanorod capping molecules (CTAB); (C) the dependence of the Raman intensity of the 1265 cm^{-1} band on the angle. The angle is defined as the relative angle from the position at which CTAB shows the strongest intensity.

peak at 1130 cm^{-1}, which is assigned to the $\upsilon(SO_2)$ vibrations.[64]

The SERS of the antibody conjugated gold nanorods on the cancer cells in Figure 5E shows combined signals from the CTAB capping molecules, PSS bridging molecules, and antibody molecules. The CTAB still gives strong SERS peaks, suggesting that its binding to the rods does not change by adding the antibody. For the PSS bridging layer, the strongest peak in the pure powder sample at 1130 cm^{-1} is observed as a shoulder close to the CTAB $\upsilon_{sym}(C-C)$ vibrations at 1140 cm^{-1}. Other Raman peaks in the pure PSS are not enhanced, suggesting that their corresponding bonds are shielded from the rod surface by the CTAB. The cell bound anti-EGFR shows a peak at 655 cm^{-1}, which is blue-shifted by 15 cm^{-1} from the vibration of the antibody adsorbed onto the gold nanorods. This could be due to the change in the strength of the surface plasmon field around the C−S bond of the anti-EGFR as a result of its binding to the cancer cell EGFR. The glycine peak at 896 cm^{-1} of the antibodies is shown as a weak peak at 893 cm^{-1} after cell binding.

Figure 5E also shows that several new peaks appear after the incubation of the antibody/Au conjugates with cancer cells. These are 712, 851, and 1238 cm^{-1}. The 712 cm^{-1} could be from the deformation vibrations of COO^- of the proteins[62] in the antibody or EGFR itself. The 851 cm^{-1} could possibly be from the tyrosine ring breathing vibration,[61−63,65−67] and the 1238 cm^{-1} could be from the tryptophan ring vibrations.[61,67,68] The appearance of those peaks when the anti-EGFR/gold nanorods are adsorbed onto cancer cells is probably due to the enhanced surface plasmon field resulting from the aggregated configuration of the assembled rods on the cancer cell surface. These bands could be from the protein molecules of the anti-EGFR antibody and/or EGFR itself. We cannot distinguish at this time. The surface plasmon fields can be felt for large distances away from the particles themselves.

In summary, by using light scattering imaging and microabsorption spectroscopy, it is found that the gold nanorods conjugated to anti-EGFR monoclonal antibodies are homogeneously aligned in their binding to the cancer cell surface due to the overexpression of EGFR on the cancer cell surface. The Raman band at 1265 cm^{-1} of the CTAB molecules, which cap the nanorods bound to the cancer cells, shows a strong polarization character. This is due to the anisotropic alignment of the assembled gold nanorods with respect to the cell surface and resulting from the binding of the antibody to the overexpressed EGFR on the surface of

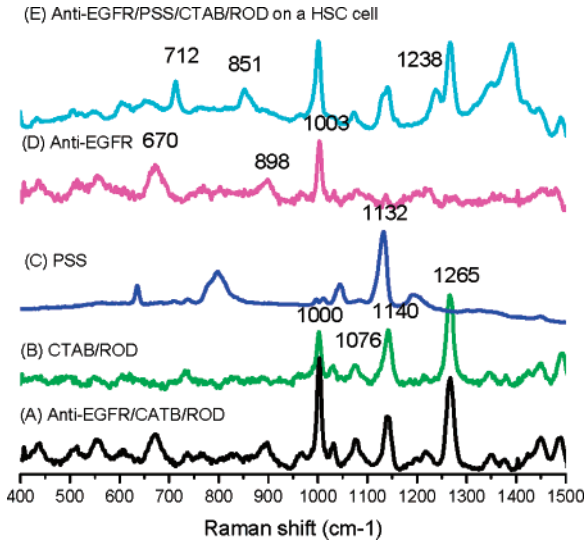

Figure 5. SERS of the individual and the final combined system: (A) SERS of anti-EGFR antibody adsorbed on CTAB capped gold nanorods; (B) SERS of CTAB capping molecules on gold nanorods; (C) Raman spectrum of poly(styrenesulfonate) powder; (D) SERS of anti-EGFR signals by subtracting (B) from (A); (E) SERS of the anti-EGFR antibody conjugated gold nanorods on a HSC cancer cell.

the cancer cells. Thus the cancer cell is able to align the gold nanorods on its surface, resulting in strong anisotropic but homogeneous electromagnetic fields that are utilized for surface enhanced, sharp, and well resolved Raman scattering spectra. Identification of this strongly enhanced Raman scattering due to aligned nanorod arrays represents a molecular signature unique to cancer. These important spectroscopic fingerprints observed by using gold nanorods extend the important uses of gold nanorods in bioimaging and cancer biodiagnostics.

Acknowledgment. M.A.E. thanks the Miller Foundation at the University of California at Berkeley for their hospitality during his tenure as a Miller visiting professor. We thank Professor Paul Edmonds for the use of his cell culture facilities and Professor Mohan Srinivasarao for the use of his micro-absorption and micro-Raman spectrometers. We like to thank the support of the Department of Energy (grant no. DE-FG02-97ER14799) and NCI Center of Cancer Nanotechnology Excellence (CCNE) Award (U54CA119338).

References

(1) Gans, R. *Ann. Phys.* **1915**, *47*, 270−284.
(2) Papavassiliou, G. C. *Prog. Solid State Chem.* **1979**, *12*, 185−271.
(3) Bohren, C. F.; Huffman, D. R. *Absorption and Scattering of Light by Small Particles*; John Wiley: New York, 1983.
(4) Link, S.; Mohamed, M. B.; El-Sayed, M. A. *J. Phys. Chem. B* **1999**, *103*, 3073−3077.
(5) Link, S.; El-Sayed, M. A. *J. Phys. Chem. B* **2005**, *109*, 10531−10532.
(6) Link, S.; El-Sayed, M. A. *J. Phys. Chem. B* **1999**, *103*, 8410−8426.
(7) Link, S.; El-Sayed, M. A. *Int. Rev. Phys. Chem.* **2000**, *19*, 409−453.
(8) Lee, K. S.; El-Sayed, M. A. *J. Phys. Chem. B* **2006**, *110*, 19220−19225.
(9) Alekseeva, A. V.; Bogatyrev, V. A.; Dykman, L. A.; Khlebtsov, B. N.; Trachuk, L. A.; Melnikov, A. G.; Khlebtsov, N. G. *Appl. Opt.* **2005**, *44*, 6285−6295.
(10) Yu, C.; Irudayaraj, J. *Anal. Chem.* **2007**, *79*, 572−579.
(11) Huang, X.; El-Sayed, I. H.; Qian, W.; El-Sayed, M. A. *J. Am. Chem. Soc.* **2006**, *128*, 2115−2120.
(12) Wang, H.; Huff, T. B.; Zweifel, D. A.; He, W.; Low, P. S.; Wei, A.; Cheng, J. X. *Proc. Natl. Acad. Sci. U.S.A.* **2005**, *102*, 15752−15756.
(13) Oldenburg, A. L.; Hansen, M. N.; Zweifel, D. A.; Wei, A.; Boppart, S. A. *Opt. Express* **2006**, *14*, 6724−6738.
(14) Takahashi, H.; Niidome, T.; Nariai, A.; Niidome, Y.; Yamada, S. *Nanotechnology* **2006**, *17*, 4431−4435.
(15) Takahashi, H.; Niidome, T.; Nariai, A.; Niidome, Y.; Yamada, S. *Chem. Lett.* **2006**, *35*, 500−501.
(16) Huff, T.B.; Tong, L.; Zhao, Y.; Hansen, M. N.; Cheng, J. X.; Wei. A. *Nanomedicine* **2007**, *2*, 125−132.
(17) Nikoobakht, B.; Wang, J.; El-Sayed, M. A. *Chem. Phys. Lett.* **2002**, *366*, 17−23.
(18) Nikoobakht, B.; El-Sayed, M. A. *J. Phys. Chem. A* **2003**, *107*, 3372−3378.
(19) Gole, A.; Orendorff, C. J.; Murphy, C. J. *Langmuir* **2004**, *20*, 7117−7122.
(20) Suzuki, M.; Niidome, Y.; Terasaki, N.; Inoue, K.; Kuwahara, Y.; Yamada, S. *Jpn. J. Appl. Phys. B* **2004**, *43*, L554−L556.
(21) Laurent, G.; Félidj, N.; Aubard, J.; Lévia, G.; Krenn, J. R.; Hohenau, A.; Schider, G.; Leitner, A.; Aussenegg, F. R. *Phys. Rev. B* **2005**, *71*, 045430−045437.
(22) Laurent, G.; Félidj, N.; Aubard, J.; Lévia, G.; Krenn, J. R.; Hohenau, A.; Schider, G.; Leitner, A.; Aussenegg, F. R. *J. Chem. Phys.* **2005**, *122*, 011102−011105.
(23) Félidj, N.; Laurent, G.; Grand, J.; Aubard, J.; Lévi, G.; Hohenau, A.; Aussenegg, F. R.; Krenn, J. R. *Plasmonics* **2006**, *1*, 35−39.
(24) Orendorff, C. J.; Gearheart, L.; Jana, N. R.; Murphy, C. *J. Phys. Chem. Chem. Phys.* **2006**, *8*, 165−170.
(25) Yu, Yu. Y.; Chang, S. S.; Lee, C. L.; Wang, C. R. C. *J. Phys. Chem. B* **1997**, *101*, 6661−6664.
(26) Jana, N. R.; Gearheart, L.; Murphy, C. J. *J. Phys. Chem. B* **2001**, *105*, 4065−4067.
(27) Nikoobakht, B.; El-Sayed, M. A. *Chem. Mater.* **2003**, *15*, 1957−1962.
(28) Wang, Z. L.; Mohamed, M. B.; Link, S.; El-Sayed, M. A. *Surf. Sci.* **1999**, *440*, L809−L814.
(29) Wang, Z. L.; Gao, R. P.; Nikoobakht, B.; El-Sayed, M. A. *J. Phys. Chem. B* **2000**, *104*, 5417−5420.
(30) Schatza, G. C. *Acc. Chem. Phys.* **1984**, *17*, 370−376.
(31) Hao, G.; Schatz, G. C. *J. Chem. Phys.* **2004**, *120*, 357−366.
(32) Nikoobakht, B.; Wang, Z. L.; El-Sayed, M. A. *J. Phys. Chem. B* **2000**, *104*, 8635−8640.
(33) Dujardin, E.; Hsin, L. B.; Wang, C. R. C.; Mann, S. *Chem. Commun.* **2001**, 1264−1265.
(34) Jana, N. R.; Gearheart, L. A.; Obare, S. O.; Johnson, C. J.; Edler, K. J.; Mann, S.; Murphy, C. J. *J. Mater. Chem.* **2002**, *12*, 2909−2912.
(35) Caswell, K. K.; Wilson, J. N.; Bunz, U. H. F.; Murphy, C. J. *J. Am. Chem. Soc.* **2003**, *125*, 13914−13915.
(36) Chang, J. Y.; Wu, H.; Chen, H.; Ling, Y. C.; Tan, W. *Chem. Commun.* **2005**, 1092−1094.
(37) Maxwell, D. J.; Nie, S. *Proc. SPIE−Int. Soc. Opt. Eng.* **2001**, *4258*, 55−62.
(38) Jiang, J.; Bosnick, K.; Maillard, M.; Brus, L. *J. Phys. Chem. B* **2003**, *107*, 9964−9971.
(39) Schwartzberg, A. M.; Grant, C. D.; Wolcott, A.; Talley, C. E.; Huser, T. R.; Bogomolni, R.; Zhang, J. Z. *J. Phys. Chem. B* **2004**, *10*, 19191−19197.
(40) Futamata, M. *Faraday Discuss.* **2006**, *132*, 45−61.
(41) Nie, S.; Emory, S. R. *Science* **1997**, *275*, 1102−1106.
(42) Fleischmann, M.; Hendra, P. J.; Mcquillan, A. J. *Chem. Phys. Lett.* **1974**, *26*, 163−166.
(43) Jeanmaire, D. L.; Van Duyne, R. P. *J. Electroanal. Chem.* **1977**, *84*, 1−20.
(44) Albrecht, M. G.; Creighton, J. A. *J. Am. Chem. Soc.* **1977**, *99*, 5215−5217.
(45) Nabiev, I.; Morjani, H.; Manfait, M. *Eur. Biophys. J.* **1991**, *19*, 311−316.
(46) Manfait, M.; Morjani, H.; Nabiev, I. *J. Cell. Pharmacol.* **1992**, *3*, 120−125.
(47) Morjani, H.; Riou, J. F.; Nabiev, I.; Lavelle, F.; Manfait, M. *Cancer Res.* **1993**, *53*, 4784−4790.
(48) Kneipp, K.; Haka, A. S.; Kneipp, H.; Badizadegan, K.; Yoshizawa, N.; Boone, C.; Shafer-Peltier, K. E.; Motz, J. T.; Dasari, R. R.; Feld, M. S. *Appl. Spectrosc.* **2002**, *56*, 150−154.

(49) Kneipp, J.; Kneipp, H.; Rice, W. L.; Kneipp, K. *Anal. Chem.* **2005**, *77*, 2381−2385.
(50) Gittins, D. I.; Caruso, F. *J. Phys. Chem. B* **2001**, *105*, 6846−6852.
(51) Caruso, F.; Niikura, K.; Furlong, D. N.; Okahata, Y. *Langmuir* **1997**, *13*, 3427−3433.
(52) Ai, H.; Fang, M.; Jones, S. A.; Lvov, Y. M. *Biomacromolecules* **2002**, *3*, 560−564.
(53) Wiley, H. S. *J. Cell. Physiol.* **1988**, *107*, 801−810.
(54) Sako, Y.; Minoguchi, S.; Yanagida, T. *Nat. Cell Biol.* **2000**, *2*, 168−172.
(55) Sawano, A.; Takayama, S.; Matsuda, M.; Miyawaki, A. *Dev. Cell* **2002**, *3*, 245−257.
(56) Zidovetzki, R.; Yarden, Y.; Schlessinger, J.; Jovin, T. M. *Proc. Natl. Acad. Sci. U.S.A.* **1981**, *78*, 6981−6985.
(57) Ogiso, H.; Ishitani, R.; Nureki, O.; Fukai, S.; Yamanaka, M.; Kim, J. H.; Saito, K.; Sakamoto, A.; Inoue, M.; Shirouzu, M.; Yokoyama, S. *Cell* **2002**, *110*, 775−787.
(58) Clayton, A. H.; Walker, F.; Orchard, S. G.; Henderson, C.; Fuchs, D.; Rothacker, J.; Nice, E. C.; Burgess, A. W. *J. Biol. Chem.* **2005**, *280*, 30392−30399.
(59) Bryant, M. A.; Pemberton, J. E. *J. Am. Chem. Soc.* **1991**, *113*, 8284−8293.
(60) Orendorff, C. J.; Gole, A.; Sau, T. K.; Murphy, C. *J. Anal. Chem.* **2005**, *77*, 3261−3266.
(61) Grabbet, E. S.; Buck, R. P. *J. Am. Chem. Soc.* **1989**, *111*, 8362−8366.
(62) Stewart, S.; Fredericks, P. M. *Spectrochim. Acta, Part A* **1999**, *55*, 1641−1660.
(63) Podstawka, E.; Ozaki, Y.; Proniewicz, L. M. *Appl. Spectrosc.* **2004**, *58*, 570−580.
(64) Dong, W. F.; Sukhorukov, G. B.; Möhwald, H. *Phys. Chem. Chem. Phys* **2003**, *5*, 3003−3012.
(65) Peticolas, W. L.; Patapoff, T. W.; Thomas, G. A.; Postlewait, J.; Powell, J. W. *J Raman Spectrosc.* **1996**, *27*, 571−578.
(66) Naumann, D. *Appl. Spectrosc. Rev.* **2001**, *36*, 239−298.
(67) Rava, R. P.; Spiro, T. G. *J. Phys. Chem.* **1985**, *89*, 1856−1859.
(68) Chumanov, G. D.; Efremov, R. G.; Nabiev, I. R. *J Raman Spectrosc.* **1989**, *381*, 43−48.
(69) El-Sayed, I. H.; Huang, X.; El-Sayed, M. A. *Nano Lett.* **2005**, *5*, 829−834.

NL070472C